

Research Paper

Tool Path Planning for Five-Axis End Milling of Cycloidal Gears and Its Full Tooth Profile Accuracy Measurement

Jian WANG¹*, Longxing LIAO²), Shanming LUO³), Jingyu MO⁴)

¹) *School of Mechanical Engineering, Nanjing Institute of Technology*
Nanjing, 211167, China

²) *School of Mechanical Engineering, Dalian University of Science and Technology*
Dalian, 116024, China

³) *School of Mechanical and Energy Engineering, Jimei University*
Xiamen, 361021, China

⁴) *School of Aerospace Engineering, Xiamen University*
Xiamen, 361005, China

*Corresponding Author e-mail: xmwjian@163.com

This paper proposes a method of end milling of cycloidal gears using a five-axis computer analytical control (CNC) machine tool. Firstly, the basic principle of the five-axis end milling of cycloidal gears is introduced. The cutting characteristics of the ball-end and the flat-end cutters are analyzed. Secondly, the path planning method of the five-axis end milling of cycloidal gears is researched. A curvature matching method is used to check for local over-cut interference and a minimum distance method is used to check for global collision interference. These two interferences are avoided by calculating the feasible range of cutter orientations and adjusting the dips of cutter shafts. Tests of end milling of cycloidal gears are carried out using a ball-end cutter and a flat-end cutter, respectively. Finally, full tooth profile accuracy measurements are undertaken with an image-measuring instrument to assess the quality of cycloidal gears processed in this way. This study provides a theoretical basis for the improvement of the tooth profile accuracy and surface quality of cycloidal gears.

Keywords: cycloidal gear; end milling; five-axis CNC machine tool; tooth path planning; full tooth profile accuracy measurement.

1. INTRODUCTION

At present, cycloidal grinding machines are most commonly used for fine machining the tooth surfaces of cycloidal gears. Because the actual tooth profile of the cycloidal gear is usually very small, and the contour evolution typically

possesses the characteristics of a planetary transmission, it is hard to guarantee the tooth profile accuracy and the surface quality of the processed cycloidal gear. This, in turn, affects the transmission accuracy and the stability and service life of the cycloidal pinwheel speed reducer [1, 2]. To tackle this problem, this paper proposed a method of end milling of cycloidal gears using the five-axis CNC machine tool. Five-axis end milling refers to a machining method for processing cycloidal gears on a five-axis CNC machine tool by controlling the inclination of the cutter shaft and by making the outer circular arc of the cutting edge the main cutting edge.

Efficient and precise machining of gears has become a priority issue for research in the gear studies. ZHOU *et al.* [3] proposed an error compensation method for the problem that the relative position and orientation deviation of the grinding wheel and the workpiece affect the machining accuracy of five-axis CNC tooth profile grinding, and verified the effectiveness of the method through tests. ZHANG *et al.* [4] solved the problem of interference between the conical grinding tool and non-grinding flanks by using a conical grinding tool to replace the blade on the face-hobbing cutter head, and realized the fine grinding of hypoid gears. ÖZEL [5] studied the CNC milling of spur gears on a vertical machining center, and the geometric manufacturing accuracy of the gear was also discussed. BO *et al.* [6] proposed a new method of double-flank milling for face gear machining, which uses the shape of the milling tool as a free parameter to achieve efficient machining of face gears. Compared with the grinding process, the CNC machining process has high manufacturing flexibility and low production costs. However, when multi-axis CNC machine tools are used to machine complex surfaces, the rationality of the tool path planning can directly affect the processing efficiency and quality of the parts.

A lot of research has been devoted to the proper planning of the tool path. LU and WANG [7] considered the effects of geometric deviations and tangential constraints on machining quality and proposed a smoothing method for flank milling tool path planning. WU *et al.* [8] proposed an analytical model of effective cutting shape for the flat-end cutter, which is suitable for computing machining strip width. TANG [9] summarized the methods to solve the collision detection and avoidance problems in five-axis NC machining, and made a comparative analysis of their advantages and disadvantages. This then provided a means of studying ways of checking and avoiding interference. LI *et al.* [10] proposed a tracking-based numerical algorithm for the five-axis machining of the conical ball-end cutter, which reduces the computing time and improves the machining accuracy. BAJIĆ *et al.* [11] studied the effects of cutting speed, feed per tooth, and depth of cut on surface roughness, cutter wear and cutting force based on off-line processing control methods. SUN *et al.* [12] proposed a method based on planar development to generate an offset path parallel to the machining

contour. ZOU [13] proposed a novel method to generate a tool path based on 3D scanning techniques. The method transforms the tool path generation problem into a thermal diffusion problem with a robust and efficient algorithm. WU *et al.* [14] has used adjustment of the angle between the cutter and the workpiece based on the cutter shaft vector to avoid interference. WANG *et al.* [15] used a spatial three-dimensional coordinate system transformation principle to check interference, thereby adjusting the cutter position to avoid the occurrence of interference. LIU *et al.* [16] established the constraint relationship between tool axis vector and cutting force and machine tool kinematics, and obtained the feasible domain range of flank milling tool track with smooth cutting force.

Accuracy measurement for gears primarily involves special point measurements and full tooth profile measurements. Special point measurements, such as top root distance measurement and common normal line measurement can reflect the machining accuracy of a gear tooth profile to some extent but can contain significant errors. It can only assess the machining accuracy of the local tooth profile. Full tooth profile measurement encompasses both the shape of the gear tooth profile itself and the dimensional accuracy of the gear in all surrounding directions. This means it can more comprehensively reflect the processing precision of cycloidal gears. SATO *et al.* [17] proposed calibration and uncertainty evaluation methods for the single pitch deviation of gears measured using CMMs. SHI and KANG [18] and SHI *et al.* [19] proposed a concept of ‘overall error’ for gear pairs and studied the presence of an overall error in gear pairs that includes determining the tooth profile within the overall error measurement. LING *et al.* [20] analyzed the influence of probe diameter and the parameters of the positions where measurements are made when assessing gear pitch deviation and has suggested an error compensation method to assist in the conduct of such measurements. XU *et al.* [21] presented surface-profiling-based gear pitch deviation measurement for an involute spur gear. Additionally, WANG *et al.* [22] proposed a new approach to obtaining a pitch deviation evaluation index by using statistical analysis of the tooth profile deviation curve for all gears.

In summary, a lot of useful work has been carried out by researchers to solve the problem of tool interference during five-axis cutting. The key to tool path planning during five-axis CNC machining is the discrimination and avoidance of cutter interference. At present, the methods available for assessing cutter interference include direct distance methods and curvature matching methods. The main ways of avoiding such interferences are selecting an appropriate cutter size, adjusting the cutter attitude, or moving the cutter’s position. However, the amount of research on the five-axis machining of cycloid gear is relatively small, especially in the five-axis end-milling cycloidal gear process and tool path planning.

In this paper, a method of tool path planning for end milling cycloid gears using five-axis CNC machine tools is proposed. We compare the curvature of a cutter's scanning surface and the cycloidal gear tooth profile to check whether local over-cut interference is occurring. By calculating the distance from the tooth profile of the cycloidal gear to the cutter shaft, it can be checked whether global interference is occurring. Interference can then be avoided by adjusting the dips of cutter shafts. To further assist in processing cycloidal gears, we also propose an approach to obtain full tooth profile accuracy measurements by using image-measuring instruments. Our contributions can be summarized as follows:

- 1) The end milling of cycloid gears is proposed, which can realize flexible machining of the gear.
- 2) The tool path planning method for cycloid gear machining is proposed, which can directly identify the interference problem in cycloid gear end milling.
- 3) The fabricated gear is measured and evaluated with image measuring equipment that provides a way to measure this type of gear.

2. THE PRINCIPLES OF CYCLOIDAL GEAR FIVE-AXIS END MILLING

According to the different main cutting edges used by the cutters, milling can be divided into flank milling and end milling. Flank milling is performed by the side edge of the cutter. As shown in Fig. 1a, this method results in uneven stress across the various parts of the cutter, which can lead to cutter deformation, large amounts of vibration and low machining quality. End milling is performed using the outer arc cutting edge of the cutter as the main cutting edge. Milling cutters are primarily subjected to axial force during end milling, so the radial deformation and radial runout are very small. Therefore, the fine machining of the tooth surface of the cycloidal gears is performed by end milling on a five-axis CNC machine. The basic principles of the machining are shown in Fig. 1b. It can be seen that, for the end milling of the cycloidal gear in this case, the cutter is inclined at an angle with respect to the end surface of the cycloidal gear, with the cutter reciprocating linearly along the tooth profile of the cycloidal gear

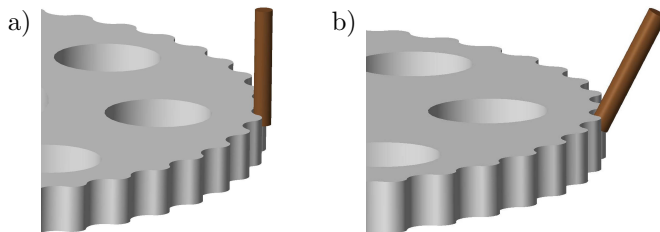


FIG. 1. Principle of flank milling and end milling: a) flank milling, b) end milling.

while rotating at high speed. The cycloid profile is cut by the outer arc cutting edge of the cutter to form a tool path similar to a line cutting process. This method can overcome the problems of large axial deformation during slotting, and large radial deformation during flank milling. Thus, it is generally beneficial for machining precision and the surface quality of the cycloidal gear.

When machining complex surfaces on CNC machines, the most commonly used cutters are ball-end cutters and flat-bottom cutters. As shown in Fig. 2a, when a complex curved surface is processed by a ball-end cutter, the blade edge is distributed across the spherical surface and the line cutting speed at each point on the spherical surface is linear to its distance from the cutter shaft. This leads to a differential distribution of power to the point during the removal of material. By contrast, flat-end cutters have a simple structure, with the working part of the cutting edge being the outer circumference of the end face. As shown in Fig. 2b, the cutting speed is constant and able to operate at its maximum at each cutting edge, ensuring a generally effective dynamic performance. In addition, in terms of the residual amount left on the surface of the workpiece after processing, there is much less left by a flat-end cutter (i.e., a smaller residual height h) than by a ball-end cutter, taking all other parameters such as cutter size and path length L to be the same, as shown in Fig. 3. But the obvious

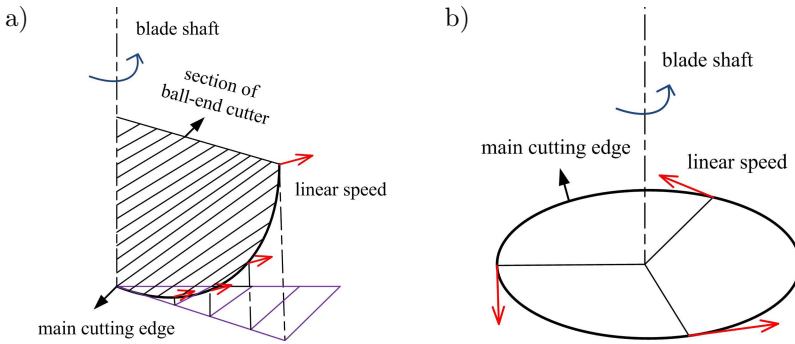


FIG. 2. Line cutting speed: a) ball-end cutter, b) flat-end cutter.

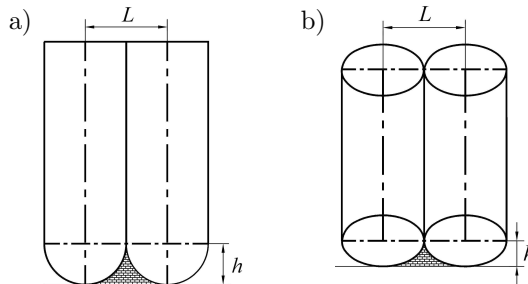


FIG. 3. Residual amount after processing: a) ball-end cutter, b) flat-end cutter.

disadvantage is that the cutter wear is severe when machining with a flat-end cutter. This will affect the cutting accuracy and surface quality. In summary, there are advantages and disadvantages to both cutters. In order to assess the machining quality, tests of end milling of cycloidal gears are carried out using a ball-end cutter and a flat-end cutter, respectively.

3. TOOL PATH PLANNING FOR FIVE-AXIS END MILLING OF CYCLOIDAL GEARS

Tool path planning is the process of arriving at a reasonable distribution of cutting points across a surface to be machined and setting the corresponding cutter shaft vectors. Before machining the cycloid tooth surface with end milling cutter, it is necessary to plan the tool path and calculate the feasible domain of the tool axis vector without interference. In this paper, the flat-end cutter is taken as the research object in the following discussions.

3.1. Curvature analysis of cycloid profile

The theoretical contour equation for a cycloidal gear can be explained as:

$$(3.1) \quad \begin{cases} x = [r_p - r_{rp}s^{-1/2}] \cos [(1 - i^H)\phi] - [a - K_1r_{rp}s^{-1/2}] \cos i^H\phi, \\ y = [r_p - r_{rp}s^{-1/2}] \sin [(1 - i^H)\phi] + [a - K_1r_{rp}s^{-1/2}] \sin i^H\phi, \end{cases}$$

where r_p is the center circle radius of the pin tooth, r_{rp} is the pin tooth radius, ϕ is the rotation angle of the arm relative to the center vector of a pin, a is the eccentricity, and i^H is the relative gear ratio of the cycloidal gear and the corresponding pin wheel $i^H = z_p/z_c$. z_p represents the number of needle wheel teeth, z_c represents the number of cycloidal gear teeth, and K_1 represents the short amplitude coefficient where $K_1 = az_p/r_p$ and $s = 1 + K_1^2 - 2K_1 \cos \phi$.

According to the Frenet formula, the expression k_0 of the theoretical tooth profile of a cycloidal gear can be calculated as follows:

$$(3.2) \quad k_0 = \frac{K_1(z_p + 1) \cos \phi - (1 + z_p K_1^2)}{r_p(1 + K_1^2 - 2K_1 \cos \phi)^{3/2}}.$$

As the actual tooth profile of a cycloidal gear is equidistant to the inner curve of the short outer cycloid, the actual tooth profile curvature k of a cycloidal gear is

$$(3.3) \quad k = \frac{k_0}{1 + k_0 r_{rp}}.$$

The maximum curvature of the cycloid profile is highly dependent on the interference of the cutter, so it is important to analyze this curvature.

At the surface of the concave tooth profile of the cycloidal gear, the maximum value of the curvature k will be

$$(3.4) \quad k_{\max} = \frac{z_p K_1 - 1}{(1 - K_1)^2 r_p + (z_p K_1 - 1) r_{rp}}, \quad \frac{1}{z_p} < K_1 < 1.$$

At the surface of the convex tooth profile of the cycloidal gear, the maximum value of the curvature k will be

$$(3.5) \quad \begin{cases} |k_{\max}| = \frac{(1 + z_p)^{3/2}}{r_p \sqrt{27(1 - K_1^2)(z_p - 1) + r_{rp}(1 + z_p)^{3/2}}} & \text{for } \frac{z_p - 2}{2z_p - 1} < K_1 < 1, \\ |k_{\max}| = \frac{1 + z_p K_1}{(1 + K_1)^2 r_p + (1 + z_p K_1) r_{rp}} & \text{for } K_1 \leq \frac{z_p - 2}{2z_p - 1}. \end{cases}$$

3.2. Calculation of the normal curvature of the cutter

3.2.1. The local coordinate system for end milling. As shown in Fig. 4, the coordinate system $\Sigma_O(O, x, y, z)$ is the workpiece coordinate system for cycloidal gears, with O being the cycloidal gear center. $\Sigma_C(C, x_C, y_C, z_C)$ is the local coordinate system for the cutter contact point C , where C is the coordinate origin, and y_C is the normal vector in the direction of C on the surface contour, which is parallel to the y -axis. z_C is the tangent to the direction of the cutter contact trajectory and is parallel to the z -axis, i.e., the tangential direction of the feed during flat-end cutter machining. x_C is determined by y_C and z_C and is parallel to the x -axis according to the right-hand rule. The coordinate system $\Sigma_T(T, x_T, y_T, z_T)$ is the fixed-cutter coordinate system, in which the cutter core

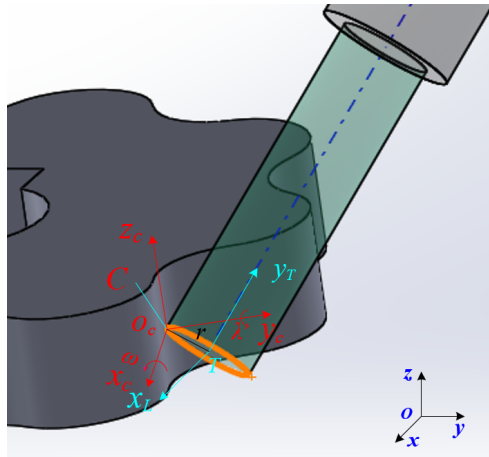


FIG. 4. End milling local coordinate system.

T is the coordinate origin, y_T is the cutter shaft direction, z_T passes through the cutter contact point, and x_T is determined by y_T and z_T according to the right-hand rule. The coordinate system Σ_T is rotated by r in the direction z_T , then rotated by the angle ω clockwise around x_C , then rotated by the angle λ clockwise around y_C to obtain the local coordinate system Σ_C , where ω is the front dip, $\omega \in [0, \pi/2]$, λ is the lateral dip, and $\lambda \in [-\pi/2, \pi/2]$.

Assuming that the cutter radius is r and the coordinate of the cutter center T under the coordinate system Σ_C is (x_T, y_T, z_T) , the coordinate vector for the cutter contact point C according to the workpiece coordinate system Σ_O will be $\mathbf{r}_C = [x_C, y_C, z_C, 1]^T$. The vector $\mathbf{r}_T = [0, 0, 0, 1]^T$ is used to represent the coordinate vector of the cutter center T in the fixed-cutter coordinate system Σ_T . Using a coordinate transformation, the coordinates of the cutter center T according to the coordinate system Σ_O can be expressed as:

$$(3.6) \quad \mathbf{O}_T = \mathbf{M}_{OT}\mathbf{r}_T = \mathbf{M}_{CT}\mathbf{M}_{OC}\mathbf{r}_T = \begin{bmatrix} r \sin \lambda \cos \omega + x_C \\ -r \sin \omega + y_C \\ r \cos \lambda \cos \omega + z_C \\ 1 \end{bmatrix},$$

where \mathbf{M}_{OT} represents the coordinate transformation matrix for transforming from Σ_T to Σ_O , and \mathbf{M}_{CT} and \mathbf{M}_{OC} represent the coordinate transformation matrices for transforming from Σ_T to Σ_C and from Σ_C to Σ_O , respectively. Their expressions are:

$$\mathbf{M}_{CT} = \begin{bmatrix} \cos \lambda & \sin \omega \sin \lambda & \cos \omega \sin \lambda & r \cos \omega \sin \lambda \\ 0 & \cos \omega & -\sin \omega & -r \sin \omega \\ -\sin \lambda & \sin \omega \cos \lambda & \cos \omega \cos \lambda & r \cos \omega \cos \lambda \\ 0 & 0 & 0 & 1 \end{bmatrix},$$

$$\mathbf{M}_{OC} = \begin{bmatrix} 1 & 0 & 0 & x_C \\ 0 & 1 & 0 & y_C \\ 0 & 0 & 1 & z_C \\ 0 & 0 & 0 & 1 \end{bmatrix}.$$

In the coordinate system Σ_T , the unit vector of the cutter shaft can be expressed as $\mathbf{y}_T = [0, 1, 0, 0]^T$ and this can be converted to the coordinate system Σ_O . In that case, the following expression will be obtained:

$$(3.7) \quad \mathbf{K}_T = \mathbf{M}_{OT}\mathbf{y}_T = \begin{bmatrix} \sin \lambda \sin \omega \\ \cos \omega \\ \cos \lambda \sin \omega \\ 0 \end{bmatrix}.$$

If b is used to represent the variable parameter of the length of the cutter shaft, the radial value of the cutter shaft can be expressed as:

$$(3.8) \quad \mathbf{R}_b = \mathbf{O}_T + b\mathbf{K}_T.$$

3.2.2. *Normal curvature.* The radial vector of the end face of the flat-end cutter in the coordinate system Σ_T can be expressed as:

$$(3.9) \quad \mathbb{R}_T = \begin{bmatrix} r \sin \theta \\ 0 \\ r \cos \theta \\ 1 \end{bmatrix}.$$

Using a coordinate transformation, the radial direction of the cutting edge of the flat-end cutter in the workpiece coordinate system Σ_O will be

$$(3.10) \quad \mathbf{R} = \mathbf{M}_{OT}\mathbf{r}_T = \begin{bmatrix} r \sin \lambda \cos \omega(1 + \cos \theta) + r \cos \lambda \sin \theta \\ -r \sin \omega(1 + \cos \theta) \\ r \cos \lambda \cos \omega(1 + \cos \theta) - r \sin \lambda \sin \theta \\ 1 \end{bmatrix} + \mathbf{r}_C.$$

The curved scanning surface V of the cutting edge of the flat-end cutter can be expressed as:

$$(3.11) \quad \mathbf{V}(t, \theta) = [r \sin \lambda \cos \omega(\cos \theta + 1) + r \cos \lambda \sin \theta] \mathbf{x} + [-r \sin \omega(\cos \theta + 1)] \mathbf{y} \\ + [r \cos \lambda \cos \omega(\cos \theta + 1) - r \sin \lambda \sin \theta] \mathbf{z} + \mathbf{r}_C.$$

The second-order partial derivative of Eq. (3.11) gives:

$$\mathbf{V}_{tt}(t, \theta) |_{\theta=\pi} = r_{ctt},$$

$$\mathbf{V}_{t\theta}(t, \theta) |_{\theta=\pi} = -(\mathbf{x})_t r \cos \lambda + \lambda_t \sin \lambda x + (\mathbf{z})_t r \sin \lambda + \lambda_t \cos \lambda z,$$

$$\mathbf{V}_{\theta\theta}(t, \theta) |_{\theta=\pi} = r \sin \lambda \cos \omega \mathbf{x} - r \sin \omega \mathbf{y} + r \cos \lambda \cos \omega \mathbf{z}.$$

If we let $\mathbf{S}(u, v)$ denote the cycloidal gear tooth profile surface, the following expression can be obtained by differential geometry:

$$\mathbf{n} = \mathbf{S}_u \times \mathbf{S}_v,$$

$$\mathbf{r}_{ct} = \frac{\partial \mathbf{S}}{\partial u} u_t + \frac{\partial \mathbf{S}}{\partial v} v_t,$$

$$\mathbf{r}_{ctt} = \frac{\partial^2 \mathbf{S}}{\partial u^2} u_t^2 + \frac{\partial^2 \mathbf{S}}{\partial v \partial u} u_t v_t + \frac{\partial^2 \mathbf{S}}{\partial v^2} v_t^2 + \frac{\partial \mathbf{S}}{\partial u} u_{tt} + \frac{\partial \mathbf{S}}{\partial v} v_{tt}.$$

According to [23], the normal curvature of the tooth profile surface can be expressed as:

$$(3.12) \quad k_1 = \frac{\mathbf{n} \cdot \mathbf{r}_{ctt}}{\mathbf{r}_{ctt} \cdot \mathbf{r}_{ct}}.$$

In Fig. 5, $C-x_C z_C$ indicates the cutting plane of the cutter scanning surface, and α and β express, respectively, the angle between the cutting direction z_C at the cutter contact point C and any direction z_α in the cutter scanning plane and the main direction t_{\min} of the minimum curvature of the cycloidal gear tooth profile. Thus, any direction in the scanning plane of the flat-end cutter can be expressed as:

$$(3.13) \quad \mathbf{z}_\alpha = \mathbf{z}_C \cos \alpha + \mathbf{x}_C \sin \alpha.$$

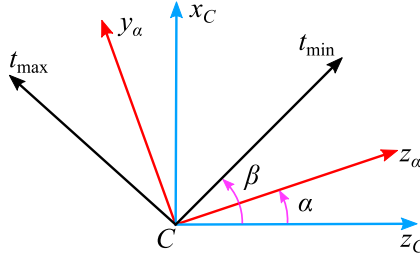


FIG. 5. Direction of the cutting plane.

The normal curvature k_α in the direction of the scanning plane of the cutting edge of the flat-end cutter z_α can be determined based on Eqs. (3.11) and (3.12), and they have:

$$(3.14) \quad k_\alpha = \frac{\sin^2 \alpha}{\cos^2 \lambda} \left(\frac{\sin \omega}{r} - k_1 \right) + k_1 - \frac{2 \cos(\alpha - \lambda) \sin \alpha}{\cos \lambda} (k_{\max} - k_{\min}) \sin 2\beta,$$

where at the cutter's point of contact, the maximum and minimum curvatures of the cycloidal gear tooth profile are k_{\max} and k_{\min} , respectively.

3.3. Interference discrimination and avoidance

The flat-end milling interference of cycloid gears can be divided into two types: global collision interference and local overcutting interference. Global collision interference refers to the collision of the cutter handle or cutter holding device with the workpiece during machining (see Fig. 6), which can be avoided by adjusting the cutter attitude. Local over-cut interference refers to excessive removal of the workpiece material by the cutter (see Fig. 7). There are three ways of avoiding this: by moving the cutter shaft, using a smaller cutter, or adjusting the cutter attitude.

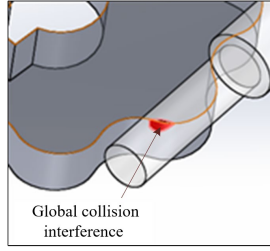


FIG. 6. Global collision interference.

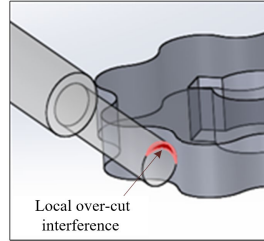


FIG. 7. Local over-cut interference.

3.3.1. *Global collision interference discrimination and avoidance.* As shown in Fig. 8, d is the distance from point P on the tooth profile surface to the cutter shaft $l_{(b)}$. And it can be expressed as:

$$(3.15) \quad d_{p,l_{(b)}} = |\mathbf{P} \times \mathbf{K}_t|,$$

where \mathbf{P} is the vector from point P on the contour surface to the center point T of the flat-end cutter, and \mathbf{K}_t is the unit vector of the cutter shaft.

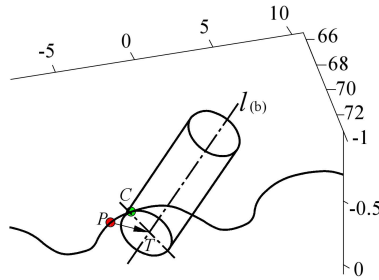


FIG. 8. Discrimination of global collision interference.

If the distance is smaller than the cutter radius, there will be a collision, and if it is larger, there will not. The minimum distance from point P to the axis $l_{(b)}$ can be expressed as:

$$(3.16) \quad d_{\min} = \min \left\{ d_{p_i, l_{(b)}} \mid i = 1, 2, \dots, n \right\} < r.$$

The tooth profile can be dissected into n points. Once the minimum distance from any point to the cutter shaft is less than the radius of the flat-end cutter, collision interference will occur. Thus, the likelihood of global collision interference can be calculated by Eqs. (3.15) and (3.16). If global collision interference occurs, the front dip ω and the lateral dip λ of the cutter can be adjusted by rotating the cutter shaft so that the distance from each point on the cycloidal gear to the cutter shaft is larger than the radius of the flat-end cutter, thereby eliminating the possibility of global collision interference.

3.3.2. Local over-cut interference discrimination and avoidance. In the z_α direction of the cutting edge of the flat-end cutter, when the cutting curvature k_α of the cutting surface is smaller than the curvature k_{\max} of the curved surface, local over-cut interference will occur. The profile of a cycloidal gear is a curved surface so the minimum curvature of the surface at the cutter contact point is $K_{\min} = 0$. Drawing upon Eqs. (3.3) and (3.14), the likelihood of local over-cut interference is as follows:

$$(3.17) \quad f(\sin \lambda, \tan \omega) = \frac{\sin \omega}{r} (1 + \tan^2 \lambda) - k_{\max} (\tan \lambda \sin \beta + \cos \beta)^2 < 0.$$

According to Eq. (3.17), when the tool radius is constant, the local over-cut interference is related to ω and λ . In other words, local over-cut interference can be avoided by selecting a suitable cutter size and adjusting the front dip ω and the lateral dip λ of the cutter.

It is worth noting that since the curvature of the convex surface of a cycloidal gear is negative, for this part of the profile, Eq. (3.17) will not hold. In other words, there is no local over-cut interference on the convex curved surface of a cycloidal gear, so local over-cut interference only needs to be considered for the concave surface.

4. FIVE-AXIS END MILLING OF CYCLOIDAL GEARS

In this section, a five-axis Vertical Machining Center DMU 40 Monoblock was used in the end milling of the cycloidal gear tooth surface. The gear material was 20CrMnTi, which was quenched after rough machining. The basic parameters of the cycloidal gear were: the number of teeth $z_c = 43$; eccentricity $a = 1.4$ mm; needle tooth radius $r_{rp} = 4$ mm; pin center circle radius $r_p = 72.5$ mm; and a short amplitude coefficient of $K_1 = 0.85$. Using Eq. (4), the radius of the curvature of the concave tooth profile was calculated to be about 4.04 mm and the radius of the curvature of the convex tooth profile was $|\rho| \approx 2.5$ mm. On the basis of these calculations, a flat-end cutter with a radius of 2 mm was selected for end milling the cycloidal tooth surface.

The cutter movement is safe when the cutter shaft is adjusted so that neither local over-cut interference nor global collision interference will occur. Drawing upon Eqs. (3.16) and (3.17), MATLAB software was used to draw a feasible operational fields for the cutter where there was no risk of global collision interference and local over-cut interference. The intersection of these fields, where no risk of either kind of interference existed, is shown in Fig. 9. The corresponding values of the front dip ω of points A , B , and C in Fig. 9 are 28° , 60.19° , and 24.07° , respectively. The corresponding values of the lateral dip λ of points A , B , and C in Fig. 9 are -8° , -33.75° , -19.49° , respectively. It can be seen that the range within which there would not be any interference was: $\lambda = [-33.75^\circ, -8^\circ]$ and $\omega = [24.07^\circ, 60.19^\circ]$. Figure 10 is a process diagram for the five-axis end milling of a cycloidal gear. Figure 11 shows a processed cycloidal gear.

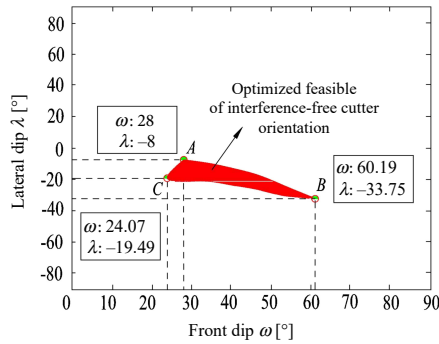


FIG. 9. The interference-free cutter attitude region.



FIG. 10. End milling process of cycloidal gears.



FIG. 11. A cycloidal gear after fine machining.

5. FULL TOOTH PROFILE ACCURACY MEASUREMENT OF CYCLOIDAL GEARS

Full tooth profile measurement of cycloid gears can help to ensure that the precision of their processing is maintained. For this study, a Hexagon Optiv Performance 442 image-measuring instrument was used to measure the full profile accuracy of the processed cycloidal gear. The device mainly consists of four segments, probe, LED, camera device and computer, as shown in Fig. 12. Specifically, the measurement process is divided into four parts as follows:

- Step 1.* The fabricated cycloidal gear is wiped with alcohol and then placed on the image-measuring machine table.
- Step 2.* In the measurement system, the CAD drawing file corresponding to the part to be measured is called the measurement reference.
- Step 3.* Determining the center of the fabricated cycloidal gear using the three-point measurement method as a reference, combined with a camera device to obtain the actual geometric parameters of the part.
- Step 4.* The theoretical and actual profile of the gear is compared to obtain the error distribution of its full tooth profile.

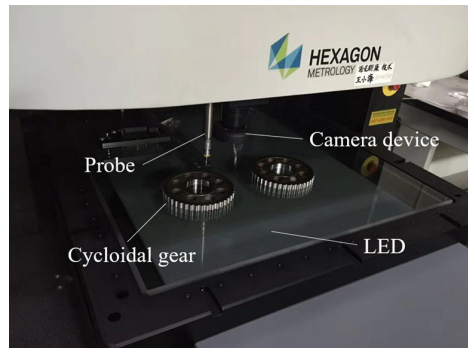


FIG. 12. Full tooth profile measurement process for cycloidal gears.

Deciding an initial measurement point on the cycloidal profile and selecting each subsequent sampling point on the contour are essential. If these are not properly selected, there will be errors in the detected results. As shown in Fig. 13, the diameter of the central circle of a cycloidal gear will pass through a tooth root at point A and a tooth top at point B . The center O of the circle can be found using the probe of the image-measuring instrument. A measurement coordinate system can be established by setting a point as the origin. The measuring instrument probe can take point A as the measurement starting point and its software will then automatically scan the points on the tooth profile to obtain the measurement data. For the convenience of observation, Fig. 13 also

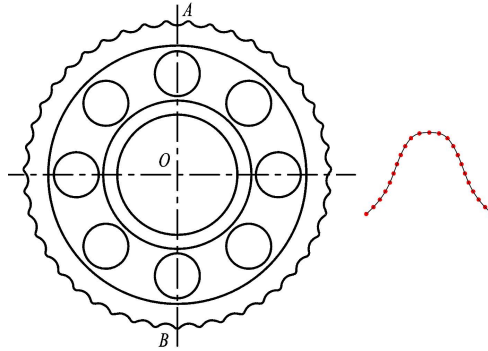


FIG. 13. Determining the starting point and sampling points for measurement.

shows a partially enlarged view of a tooth sampling point. For the entire gear, the instrument sampled a total of 5160 points.

Figure 14 shows the measurement results, indicating the accuracy of the full tooth profile. It shows the actual machining of the full tooth profile compared with the theoretical tooth profile. The yellow part is the undercut area, i.e., the uncut part. The red part is the overcut area, i.e., the part that was cut excessively. For the convenience of observation and analysis, both the overcut and undercut regions are expanded. Figure 15 is a graph of the results of the full profile measurement data. The accuracy fluctuated between -0.5 mm and $+0.3$ mm, with positive values indicating the amount of undercutting and negative values the overcutting.

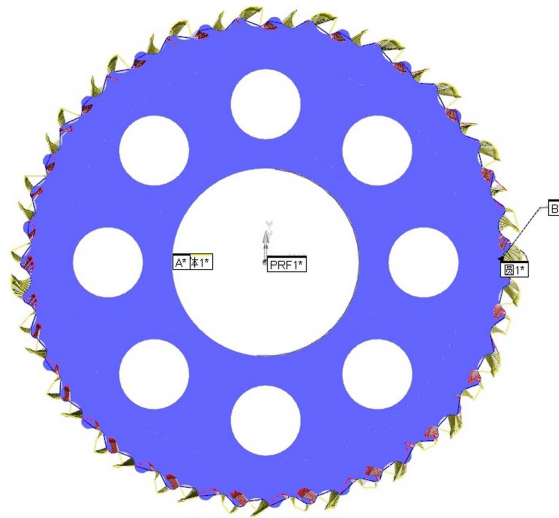


FIG. 14. The overcut and undercut areas.

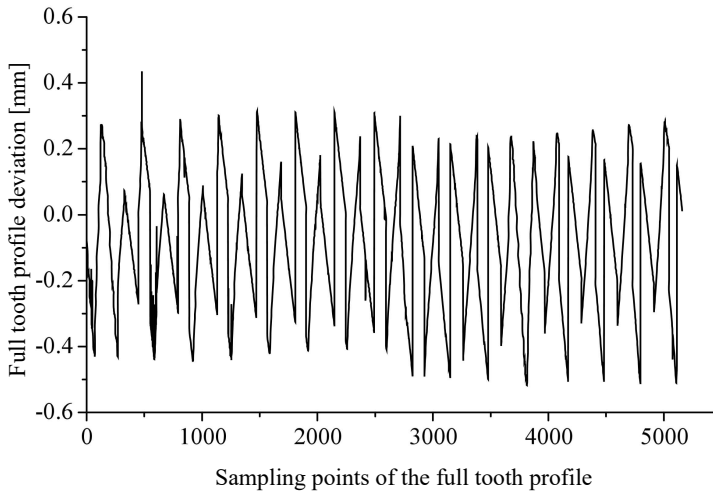


FIG. 15. Measurement results when using a flat-end cutter.

For comparison, a test of end milling of cycloidal gear using a ball-end cutter is also carried out. Figure 16 shows the accuracy measurement results for a cycloidal gear machined with a ball-end milling cutter. Here the accuracy fluctuated between 0.020 mm and 0.036 mm. So, compared to the flat-end cutter, the processing quality was significantly improved and there was almost no overcut. The main reason for this is that the cutter wear is severe when machining with a flat-end cutter. According to the cycloidal gear industrial precision standard “JB/T 104919–2005”, the processing accuracy of end milling with a ball-end milling cutter is between level 6 and level 8, with the average value being about level 7.

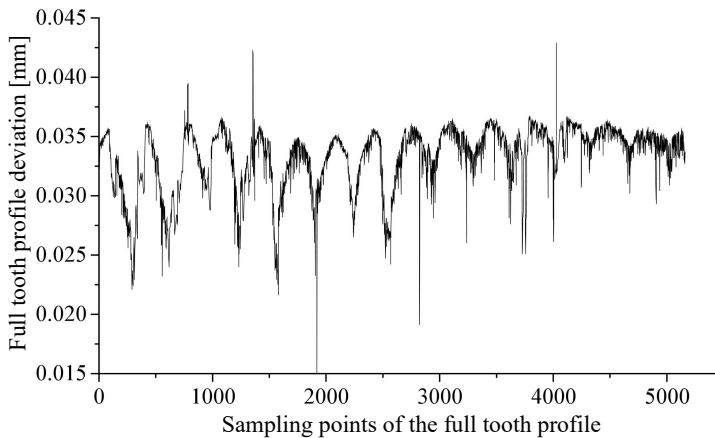


FIG. 16. Measurement results when using a ball-end milling cutter.

6. CONCLUSION

Since the machining accuracy of cycloidal gears affects the transmission accuracy, motion stability and service life of cycloidal gear speed reducers, investigating the machining method of cycloidal gears is still needed. The five-axis end milling process for cycloidal gears proposed in this paper is an attempt in this direction. In order to improve the tooth profile accuracy and surface quality, we have studied ways of approaching the tool path planning for end milling cycloid gears. A curvature matching method and a minimum distance method were proposed that can quickly and effectively check local over-cut interference and global collision interference. These two interferences are avoided by calculating the feasible range of cutter orientations and adjusting dips of cutter shafts. In order to assess the machining quality, tests of end milling of cycloidal gears are carried out using a ball-end cutter and a flat-end cutter, respectively. In this paper, we also presented a method for measuring cycloidal gear full profile accuracy by using an image-measuring instrument. The measurement result shows that the precision of the cycloidal gear machined with a ball-end cutter is between $+0.02$ mm and -0.036 mm, which is obviously better than that of the gear machined with a flat-end cutter. The preliminary results show that the method of end milling of cycloidal gears using a ball-end cutter is feasible and can meet grinding quality industrial standards.

ACKNOWLEDGMENTS

The work was supported by the National Natural Science Foundation of China under No. 51205335 and No. 52205055, and the Scientific Research for the High-Level Talent of Nanjing Institute of Technology under No. YKJ201702. These financial supports are gratefully acknowledged. The authors also sincerely appreciate the comments and modification suggestions made by the editors and anonymous referees.

REFERENCES

1. LI T., LI J., DENG X., TIAN M., LI Y., Quantitative correction method for the grinding errors of cycloidal gears in precision reducer, *Journal of Advanced Mechanical Design, Systems, and Manufacturing*, **14**(4): JAMDSM0052, 2020, doi: 10.1299/jamdsm.2020jamdsm0052.
2. JIANG C., WANG H.L., HAN T.H., LIU X., Simulation and compensation of axial geometric errors for cycloidal gears based on form grinding, *Mathematical Problems in Engineering*, **2022**: 4804498, 2022, doi: 10.1155/2022/4804498.
3. ZHOU B., WANG S., FANG C. SUN S., DAI H., Geometric error modeling and compensation for five-axis CNC gear profile grinding machine tools, *The International Journal of*

- Advanced Manufacturing Technology*, **92**(5): 2639–2652, 2017, doi: 10.1007/s00170-017-0244-y.
4. ZHANG W., WEI X., GUO X., TAN R., WANG Y., A novel continuous indexing method for face-hobbed hypoid gear tooth grinding, *Mechanism and Machine Theory*, **173**: 104826, 2022, doi: 10.1016/j.mechmach-theory.2022.104826.
 5. ÖZEL C., A study on cutting errors in the tooth profiles of the spur gears manufactured in CNC milling machine, *The International Journal of Advanced Manufacturing Technology*, **59**(1): 243–251, 2012, doi: 10.1007/s00170-011-3475-3.
 6. BO P., GONZÁLEZ H., CALLEJA A., DE LACALLE L.N.L., BARTOŇ M., 5-axis double-flank CNC machining of spiral bevel gears via custom-shaped milling tools. Part I: Modeling and simulation, *Precision Engineering*, **62**: 204–212, 2020, doi: 10.1016/j.precisioneng.2019.11.015.
 7. LU Y.-A., WANG C.-Y., Smoothing method of generating flank milling tool paths for five-axis flat-end machining considering constraints, *The International Journal of Advanced Manufacturing Technology*, **110**(11): 3295–3309, 2020, doi: 10.1007/s00170-020-05880-z.
 8. WU B., LIANG M., ZHANG Y., LUO M., TANG K., Optimization of machining strip width using effective cutting shape of flat-end cutter for five-axis free-form surface machining, *The International Journal of Advanced Manufacturing Technology*, **94**(5): 2623–2633, 2018, doi: 10.1007/s00170-017-0953-2.
 9. Tang T.D., Algorithms for collision detection and avoidance for five-axis NC machining: a state of the art review, *Computer-Aided Design*, **51**: 1–17, 2014, doi: 10.1016/j.cad.2014.02.001.
 10. LI X., REN J., TANG K., ZHOU Y., A tracking-based numerical algorithm for efficiently constructing the feasible space of tool axis of a conical ball-end cutter in five-axis machining, *Computer-Aided Design*, **117**: 102756, 2019, doi: 10.1016/j.cad.2019.102756.
 11. BAJIĆ D., CELENT L., JOZIĆ S., Modeling of the influence of cutting parameters on the surface roughness, tool wear and the cutting force in face milling in off-line process control, *Strojniški vestnik – Journal of Mechanical Engineering*, **58**(11): 673–682, 2012, doi: 10.5545/sv-jme.2012.456.
 12. SUN Y., REN F., ZHU X., GUO D., Contour-parallel offset machining for trimmed surfaces based on conformal mapping with free boundary, *The International Journal of Advanced Manufacturing Technology*, **60**(1): 261–271, 2012, doi: 10.1007/s00170-011-3577-y.
 13. ZOU Q., Robust and efficient tool path generation for machining low-quality triangular mesh surfaces, *International Journal of Production Research*, **59**(24): 7457–7467, 2021, doi: 10.1080/00207543.2020.1842939.
 14. WU B., ZHANG D., LUO M., ZHANG Y., Collision and interference correction for impeller machining with non-orthogonal four-axis machine tool, *The International Journal of Advanced Manufacturing Technology*, **68**(1): 693–700, 2013, doi: 10.1007/s00170-013-4791-6.
 15. WANG G.X., SHU Q.L., WANG J., WANG W.S., Tool interference checking for 5-axis NC machining of sculptured surfaces [in Chinese], *China Mechanical Engineering*, **25**(3): 299–303, 2014.
 16. LIU C., LI Y., JIANG X., SHAO W., Five-axis flank milling tool path generation with curvature continuity and smooth cutting force for pockets, *Chinese Journal of Aeronautics*, **33**(2): 730–739, 2020, doi: 10.1016/j.cja.2018.12.003.

17. SATO O., OSAWA S., KONDO Y., KOMORI M., TAKATSUJI T., Calibration and uncertainty evaluation of single pitch deviation by multiple-measurement technique, *Precision Engineering*, **34**(1): 156–163, 2010, doi: 10.1016/j.precisioneng.2009.05.009.
18. SHI Z.Y., KANG Y., Gear pair integrated error and its measurement method [in Chinese], *Journal of Tianjin University*, **45**(2): 128–134, 2012.
19. SHI Z.Y., WANG X.Y., YU B., SHU Z.H., New method to determine the tooth profile evaluation area in gear integrated error measurement [in Chinese], *Journal of Mechanical Engineering*, **53**(3): 34–42, 2017.
20. LING S.Y., C L.D., LOU Z.F., LIU Q., ZHAO Y.W., Error compensation of the measurement position in ultra-precision gear pitch deviation measurement [in Chinese], *Chinese Journal of Scientific Instrument*, **35**(3): 691–696, 2014.
21. XU B., SHIMIZU Y., ITO S., GAO W., Pitch deviation measurement of an involute spur gear by a rotary profiling system, *Precision Engineering*, **39**: 152–160, 2015, doi: 10.1016/j.precisioneng.2014.08.003.
22. WANG X.Y., SHI Z.Y., LIN J.C., Fast measurement method for pitch deviation based on full tooth profile information [in Chinese], *Chinese Journal of Scientific Instrument*, **37**(10): 2202–2210, 2016.
23. ZHOU J.J., *High Efficiency and Accuracy Machining of Complex Surfaces* [in Chinese], Zhejiang: Zhejiang University Press, 2014.

Received October 18, 2021; accepted version November 18, 2022.



Copyright © 2023 The Author(s).

This is an open-access article distributed under the terms of the Creative Commons Attribution-ShareAlike 4.0 International (CC BY-SA 4.0 <https://creativecommons.org/licenses/by-sa/4.0/>) which permits use, distribution, and reproduction in any medium, provided that the article is properly cited. In any case of remix, adapt, or build upon the material, the modified material must be licensed under identical terms.